THE JOURNAL OF PHYSICAL CHEMISTRY A
A JOURNAL OF THE AMERICAN CHEMICAL SOCIETY

pubs.acs.org/JPCA

Article

Multichannel Radical–Radical Reaction Dynamics of NO + Propargyl Probed by Broadband Rotational Spectroscopy

Published as part of The Journal of Physical Chemistry virtual special issue "10 Years of the ACS PHYS Astrochemistry Subdivision".

Nureshan Dias, Ranil M. Gurusinghe, and Arthur G. Suits*

Cite This: *J. Phys. Chem. A* 2022, 126, 5354–5362

Read Online

ACCESS | Metrics & More | Article Recommendations | Supporting Information

ABSTRACT: Chirped-pulse rotational spectroscopy in a quasi-uniform flow has been used to investigate the reaction dynamics of a multichannel radical–radical reaction of relevance to planetary atmospheres and combustion. In this work, the NO + propargyl (C_3H_3) reaction was found to yield six product channels containing eight detected species. These products and their branching fractions (%), are as follows: HCN (50), HCNO (18), CH_2CN (12), CH_3CN (7.4), HC_3N (6.2), HNC (2.3), CH_2CO (1.3), HCO (1.8). The results are discussed in light of previous unimolecular photodissociation studies of isoxazole and prior potential energy surface calculations of the NO + C_3H_3 system. The results also show that the product branching is strongly influenced by the excess energy of the reactant radicals. The implications of the title reaction to the planetary atmospheres, particularly to Titan, are discussed.

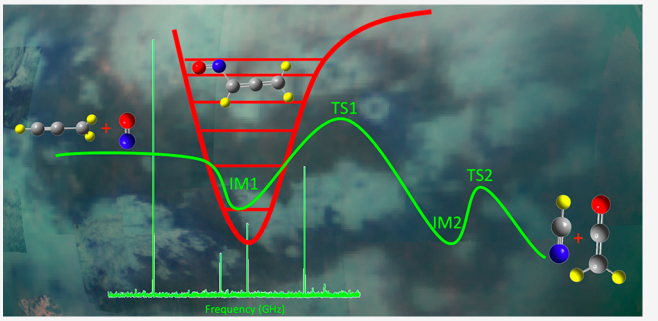

INTRODUCTION

Detailed investigations of radical reaction dynamics are crucial for understanding the microscopic mechanisms and branching of elementary reactions that occur in exotic environments such as the interstellar medium (ISM), planetary atmospheres, and high-temperature flames. However, in comparison to the study of reactions of stable closed shell molecules, little progress has been made in radical–radical systems particularly for polyatomic radicals. This is because of the challenge in producing sufficient radicals under well-defined conditions for study as well as the complex product branching for reactions initiated high on the global potential energy surface. Nonetheless, recent experimental advances in molecular beams and laser techniques have improved the ability to investigate reaction dynamics involving radicals.[1−3] Many bimolecular neutral–neutral reactions containing at least one radical reactant have been examined at high energies utilizing the crossed molecular beam approach[4−6] and at low temperatures using the CRESU approach[7−9] (French acronym meaning reaction kinetics in uniform supersonic flows). Kaiser and co-workers were the first to investigate a radical–radical reaction using a crossed molecular beam technique with mass spectrometric detection.[10] They studied the dynamics of ground state C atoms with the C_3H_3 radical at an average collision energy of 42.0 kJ mol^{-1}, and their study revealed the formation of diacetylene. Following this, many groups have examined radical–radical reactions of hydrocarbon radicals with themselves or with atoms such as H, N, O, X (=F and Cl) and other radical species involving OH, CN, NH, and C_2.[11−16] These have been performed under single collision conditions employing crossed molecular beam methods with various probe methods such as mass spectrometry and laser-induced fluorescence (LIF).[17,18]

The kinetics of neutral reactions involving radicals have been investigated at low temperatures utilizing the CRESU technique because of the importance of these reactions in astrochemical environments. This approach achieves a uniform supersonic flow by isentropically expanding a gas mixture, mostly composed of a buffer gas (He, Ne, or Ar), through a convergent–divergent Laval nozzle.[19,20] This method as well as its adaptation to study kinetics of neutral–neutral reaction have been described elsewhere.[9] Initially, numerous "prototype" radical–radical reactions were explored using this technique, with one reactant being a stable open shell molecule such as NO or O_2.[21,22] This method has since

Received: March 8, 2022
Revised: July 13, 2022
Published: August 8, 2022

https://doi.org/10.1021/acs.jpca.2c01629
J. Phys. Chem. A 2022, 126, 5354–5362

been used to explore a few reactions involving two unstable radicals. First, Sims et al. investigated the kinetics of the O + OH system at temperatures ranging from 39 to 142 K.[23] This is one of the key reactions responsible for producing molecular O_2 in the ISM, and the rate constant for this reaction is found to be fast regardless of the temperature. Following this successful attempt, several studies on radical−radical reactions have been carried out using the CRESU technique.[2,24,25]

In a radical−radical reaction, reactant molecules can combine to form a single molecular adduct that will subsequently decay, or the two radicals can undergo metathesis to form two or more products. Because collisions with the inert carrier gas greatly outnumber reactive collisions under typical experimental conditions, it is usual to presume that products formed in either of these ways are thermalized by third-body collisions. However, when these radicals are produced by laser photolysis, a significant amount of excess internal energy can be retained in the radical reactants. Thermalization of these radicals by third body collisions is inefficient. Therefore, because of this excess energy, the reactive landscape changes entirely and the reaction dynamics may yield various products with different branching ratios. This was shown in our recent investigation on the radical−radical reaction of propargyl + NH_2/ND_2.[26] In that experiment, analogous to the study presented here, the radicals were produced by the 193 nm laser photolysis of propargyl bromide and NH_3/ND_3. We estimated that the radicals were produced with at least 200 kJ mol^{-1} of excess energy. Using chirped pulse rotational spectroscopy, six distinct product channels including isomers and isotopologues were identified. Moreover, with the aid of high-level theoretical calculations, we showed that the substantial excess internal energy of the C_3H_3 and NH_2/ND_2 reactants was important to account for the bimolecular product branching. A comprehensive investigation of a similar photochemically initiated radical−radical reaction involving C_3H_3 and NO is presented here.

Photochemically initiated radical−radical reactions are important astrochemically as one of the key types of reactions that may occur in planetary atmospheres to produce complex molecular species. These reactions are typically barrierless and have very large rate coefficients even at very low temperatures, making them important to consider in cold planetary atmospheres. Many of these radical−radical reactions are discussed in relation to Titan's atmosphere because of its similarities to the prebiotic Earth and its rich hydrocarbon atmosphere. Titan's atmosphere is dominated by CH_4 and N_2 chemistry, and the Cassini−Huygens mission results confirmed that the molecular complexity in Titan's atmosphere is initiated by photodissociation and photoionization of these species to form hydrocarbons and nitrogenated compounds via neutral−neutral and ion−molecule reactions. These reactions can lead to the production of several hydrocarbons including C_3H_3, a key radical considered to be implicated in soot formation and aerosol formation on Titan. Furthermore, the most recent modeling results imply that C_3H_3 could be prevalent enough to be present in Cassini/INMS data. NO, however, is yet undetected in Titan's atmosphere.[27] However, modeling indicates that NO likely has a relatively high abundance in Titan's upper atmosphere where it is formed.[28]

Previous studies on NO + C_3H_3 have primarily focused on the formation of adducts. DeSain et al. examined this reaction as a function of temperature and pressure using infrared kinetic spectroscopy.[29] At room temperature and below, the reaction rate was found to increase with pressure, and at constant buffer gas density, the rate constant decreased with increased temperature. Their findings indicate that this reaction occurs by termolecular addition to produce C_3H_3NO. They also explored the energetics of this reaction using B3LYP/6-311++G(2df,2pd) and G2 calculations. According to these calculations, the addition of NO to the CH ("tail") end of propargyl is more exothermic than the addition to the CH_2 ("head") end. Their study further demonstrated that the weaker adduct (NO attack to the CH_2 end) does not contribute to the rate constant at low pressures but may influence the rate constant at high pressures. However, this investigation did not identify any products or branching fractions for the reaction. Wang and co-workers investigated the potential energy surface of this reaction at the CCSD(T)/cc-pVTZ//B3LYP/6-311++G (df, pd) level of theory in a subsequent theoretical investigation.[30] Three favorable channels, including the formation of two adducts and the bimolecular product channel yielding HCN and H_2CCO, were confirmed. Rate coefficients for adduct-producing channels were determined using the RRKM-CVT method with tunneling corrections at temperatures ranging from 200 to 800 K and pressures ranging from 1×10^{-4} to 10 bar. The calculated rate coefficients have a negative temperature dependence and a positive pressure dependence whereas the rate coefficients at 195 and 295 K agreed well with DeSain et al.'s previous experiment measurements.

The most comprehensive theoretical investigation on the NO/C_3H_3 system was performed by Danilack and Goldsmith, who analyzed the potential energy surface using multireference methods.[31] Their calculations showed that a significant fraction of NO/C_3H_3 is stabilized into the initial adducts at high pressures (>1 atm) and low temperatures (<900 K) and that the initial adduct nitrosoallene can be cyclized into isoxazole. The bimolecular products are then formed from the latter via the key intermediate β-formylvinylnitrene, and they discovered three major bimolecular product channels from this reaction: HCN + CH_2CO, CH_2CNH + CO, and CH_3CN + CO. These product channels are consistent with the previous studies of the unimolecular photodissociation of isoxazole. Additional RRKM/master equation calculations were performed to determine the temperature- and pressure-dependent rate constants.

In contrast to previous experimental measures for assessing the rate of the NO + C_3H_3 system, we here apply a near-universal and direct detection method that allows us to observe numerous products arising from the bimolecular reaction. We apply chirped pulse rotational spectroscopy in a pulsed flow (CPUF) to investigate the gas phase bimolecular reaction dynamics of NO + C_3H_3. In previous studies, we demonstrated the successful application of CPUF for product branching determinations in unimolecular and bimolecular reactions with isomer and vibrational level specificity, and we have recently shown application to low-temperature kinetics determination employing sampling.[32−34]

We used a helium quasi-uniform flow for this work, which has previously been characterized using both computational fluid dynamics and experimental Pitot measurements.[32] In this flow, the NO + C_3H_3 reaction is initiated by laser photolysis of propargyl bromide or 1,2-butadiene, and corresponding products are detected in the low-density (~10^{15} molecules/cm^3), low-temperature (11 K) region downstream of the flow (see Figure 1). In this work, detected products (shown in

https://doi.org/10.1021/acs.jpca.2c01629
J. Phys. Chem. A 2022, 126, 5354−5362

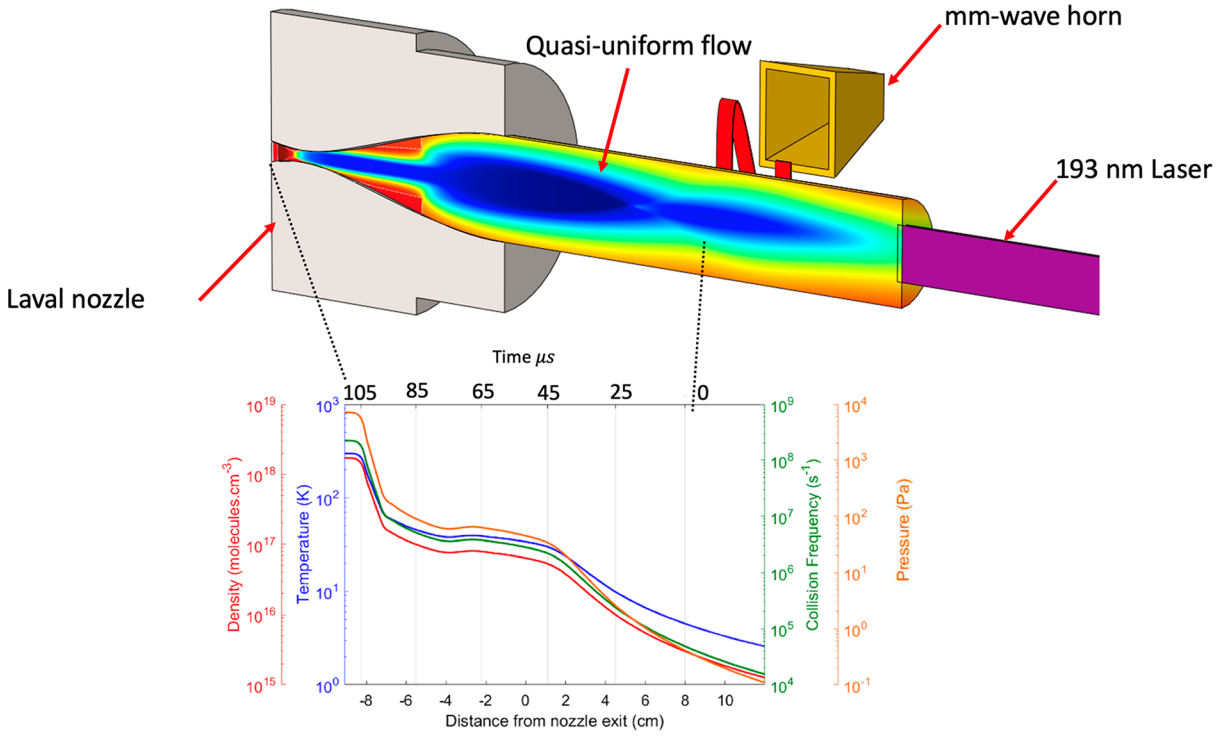

Figure 1. Schematic of the experimental setup. A high-intensity gas pulse is expanded through a Laval nozzle to generate the quasi-uniform flow. The reaction is initiated by an ArF excimer laser that enters the chamber from the back. The flow is then irradiated by a millimeter-wave pulse at 5 microsecond intervals, and the FID of the excited molecules is collected using a millimeter-wave horn and down-converted for detection and averaging. The bottom figure depicts the evolution of the various thermodynamic properties along the flow axis from fluid dynamics simulations.[32]

bold) were observed possibly associated with the following reaction channels as discussed below:

$$\mathrm{NO} + \mathrm{C_3H_3} \rightarrow \mathbf{HCN} + \mathrm{CH_2CO}$$
$$\rightarrow \mathbf{HNC} + \mathrm{CH_2CO}$$
$$\rightarrow \mathrm{CO} + \mathbf{CH_3CN}$$
$$\rightarrow \mathbf{HCO} + \mathbf{CH_2CN}$$
$$\rightarrow \mathbf{HC_3N} + \mathrm{H_2O}$$
$$\rightarrow \mathbf{HCNO} + \mathrm{HCCH}$$

However, as discussed below, we assign the HCNO product to the reaction $^3CH_2$ + NO. Normalized line intensities from rotational spectra were used to determine the product branching of each species detected. It is clear that the initial adducts are formed with high excess energy. Multiple products channels proceed from these excited intermediates. Our present findings are discussed in light of previous unimolecular photodissociation studies of isoxazole[35,36] and prior potential energy surface calculations of the NO/C_3H_3 system by Danilack and Goldsmith and by Wang et al.[30,31]

EXPERIMENTAL SECTION

The CPUF experimental setup consisting of a pulsed Laval flow coupled to a chirped pulse millimeter-wave spectrometer is discussed in our previous publications.[32,33,37] Therefore, only a brief experimental description relevant to this study is provided below. In this work, propargyl bromide (99%, Sigma-Aldrich) and 1,2-butadiene (98% Chemsampco) were used as precursor molecules for the propargyl radical. The reaction of NO with C_3H_3 (0.5% C_3H_3Br or CH_2CCHCH_3 with 0.5% NO, seeded in He) was initiated by 193 nm ArF excimer (COMPexPro) laser. Loosely focused 193 nm radiation enters from the back of the vacuum chamber and counter propagates to the quasi-uniform flow. The laser power is about 10 mJ/pulse near the nozzle throat, which corresponds to a total fluence of 5×10^{16} photons/cm^2/pulse. Initial 1 GHz broadband millimeter-wave pulses were used in the range 70−90 GHz to identify the products corresponding to the NO + C_3H_3 reaction. The individual rotational lines observed in the initial broad chirps were excited with the resonant frequency $\pi/2$ pulses of various durations, as described previously.[32] Both up-chirps and down-chirps were used to acquire the spectra recorded in this study ensuring the relative time at each $\pi/2$ pulse broadcast into the system had no little on the branching results obtained. The experiment repetition rate was 3 Hz. For each gas pulse, the millimeter-wave single frequency $\pi/2$ pulses irradiate the sample 30 times in 5 μs intervals using the fast frame capabilities of the oscilloscope. This allows us to capture the dynamics in the flow on this time scale, while also allowing us to determine the product's birthplace in the quasi-uniform flow given the flow velocity ($\approx$1600 ms^{-1}), the position of the millimeter wave horns and the product appearance time. In the current study, the millimeter-wave horns are located 8.5 cm away from the nozzle exit. The schematic of the experimental setup and the flow properties are shown in Figure 1. The characteristics of the flow were calculated using computational fluid dynamics simulations as described previously.[32] These properties were compared to experimental Pitot measurements, which showed good agreement. The laser is fired 25 μs after the first millimeter-wave pulse and corresponds to the reaction's time zero. The products start to appear around 70 μs and peak at 100 μs. As shown in Figure 1, this region corresponds to the

https://doi.org/10.1021/acs.jpca.2c01629
J. Phys. Chem. A 2022, 126, 5354−5362

transition from a 40 K uniform flow to a high-density/higher temperature portion of the flow nearer the nozzle throat. We emphasize that these are not necessarily low-temperature measurements. The extended flow permits rotational and some vibrational cooling of the products prior to the second expansion to the probed region. Time-dependent rotational spectra in the 80−92 GHz range arising from the products of the bimolecular reaction of propargyl radical with NO were obtained. From the corresponding rotational lines, the time evolution of the integrated intensities of eight separate products were obtained and the relative branching for each product was determined.

RESULTS

The propargyl radical for this study was generated from the UV photodissociation of 1,2-butadiene or propargyl bromide. The photodissociation of propargyl halides (=Cl, Br) has been investigated extensively and found to dissociate through C−X bond fission and HX elimination,[38,39] and in both cases the branching for C−X fission dominates over HX elimination. However, the photodissociation of 1,2-butadiene can occur through H loss and methyl loss.[40] Here the methyl loss channel is dominant giving propargyl radical. The internal energies of the propargyl radical obtained from both of these precursors are similar: up to 200 kJ/mol for propargyl bromide and 170 kJ/mol for 1,2-butadiene. The propargyl radical formed from either precursor can also absorb a second photon and dissociate into C_3H_2 and C_3H. The results of this second photon absorption have been examined in a separate study.[32]

Figure 2 depicts a portion of the time evolution of the rotational spectra of the products formed in the NO + C_3H_3 reaction ranging from 55 to 105 μs. Propargyl derived from both 1,2-butadiene and propargyl bromide yielded comparable results with similar time profiles. Therefore, only the data obtained from propargyl bromide are reported here. We found

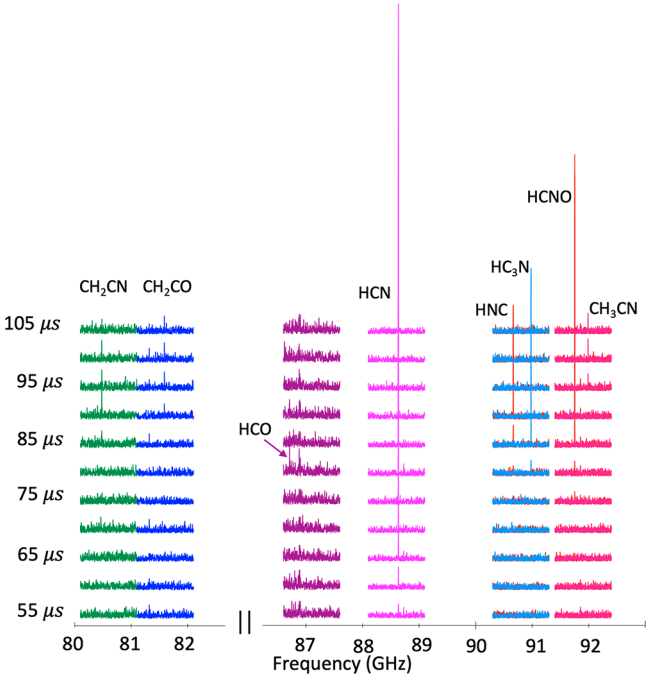

Figure 2. Time evolution spectra observed in this study. Times shown are after the laser pulse.

signals for rotational transitions of eight different products in their vibrational ground states: HCN, HNC, CH_2CO, CH_2CN, HCO, CH_3CN, HCNO, and HC_3N. We have also observed two additional transitions for vibrationally excited HCN. The millimeter-wave transition frequencies for the species discussed above have been previously assigned and were obtained from the Cologne Database for Molecular Spectroscopy (CDMS).[41]

In Figure 3a we show the time evolution of integrated intensities of products acquired in the vibrational ground state, whereas Figure 3b represents the integrated intensities of vibrationally excited HCN along with v = 0 HCN. As seen in Figure 3, nearly all the products we obtained here follow a similar trend, with products starting to appear around 70−80 μs, peaking at 100 μs, and fading away at 120 μs. According to our computational fluid dynamics simulations, these times correspond to the transition of molecules from the nearly uniform region to peak just downstream of the nozzle throat. Branching fractions were calculated using the normalized integrated intensities obtained using $\pi/2$ pulses. The signals obtained here are optimally polarized by $\pi/2$ pulses, and their coherent polarization is proportional to the population difference of the corresponding rotational levels and transition dipole moment. The total population of a species is then calculated by applying the appropriate Boltzmann weighting to the population difference and normalizing the integrated signal by transition dipole moment. A detailed description of product branching calculations is described by Broderick et al. in ref 32. The additional data required for the branching calculations such as line strength, lower state energies, and rotational partition functions were also obtained from the CDMS and summarized in Table 1. Because calculated branching fractions are sensitive to rotational temperature, the uncertainties of branching fractions were calculated with a ±3 K variation in rotational temperature in the detection region. In a separate experiment, the temperature of the detection region (11 K) was measured using propionitrile. In this study, we used six different spectra obtained at 80−105 μs after the laser to determine branching, and the results are summarized in Table 2. The variation in rotational temperature contributes the most to the uncertainty in branching, but frequency-dependent variations in sensitivity in the millilmeter-wave system could also contribute. However, we observed fairly uniform millimeter-wave power across all spectral regions, so we neglected the uncertainties associated with it.

DISCUSSION

To interpret our experimental results, we rely heavily on prior potential energy surface calculations for the C_3H_3 + NO system performed by Danilack and Goldsmith and by Wang and co-workers summarized in Figure 4. We first explore different possibilities of entrance channel attack that can occur in this reaction. For the approach of NO to C_3H_3, the N, O, or the NO π bond attack is possible. However, calculations by Wang et al., at the CCSD(T)/cc-pVTZ//B3LYP/6-311++G(df,pd) level of theory, demonstrate that only the N attack is kinetically feasible, and it can occur on either side of the C_3H_3 radical (tail, −CH end; head, $-CH_2$ end). NO addition to the head forms nitrosopropyne (IM1, $CHCCH_2NO$) and to the tail forms nitrosoallene (IM2, CH_2CCHNO). Both these adducts are formed without barriers. Their calculations further showed that nitrosoallene is about 18.9 kJ/mol more stable than the nitrosopropyne. This is consistent with Danilack and Goldsmith's computations on the same system. Furthermore,

https://doi.org/10.1021/acs.jpca.2c01629
J. Phys. Chem. A 2022, 126, 5354−5362

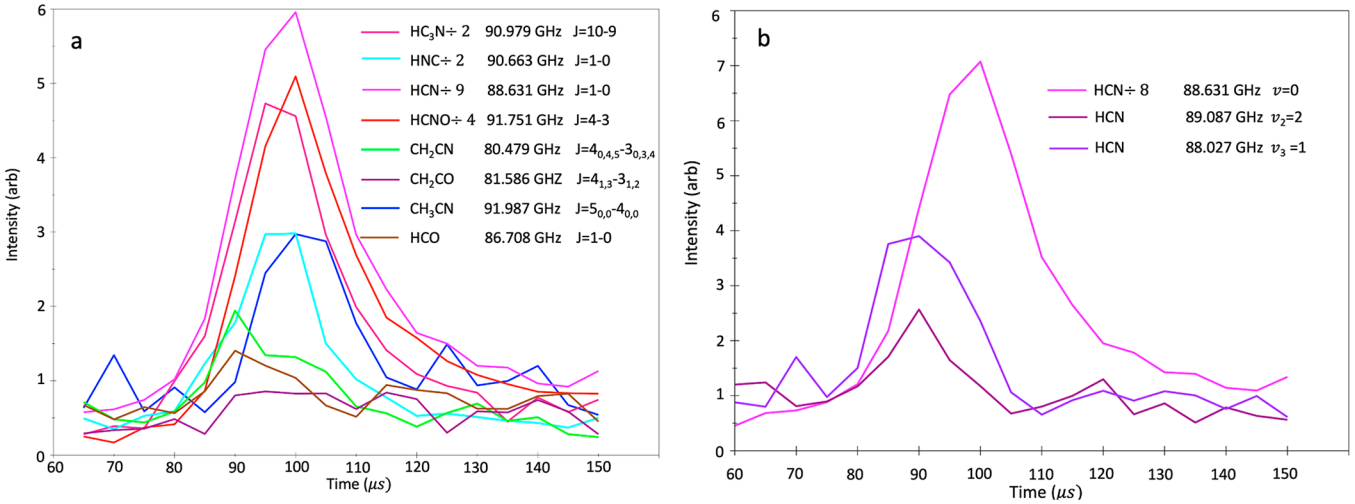

Figure 3. (a) Time evolution integrated intensities of the product observed in the bimolecular reaction of NO + C_3H_3. (b) Vibrationally excited HCN observed in this study.

Table 1. Rotational Transitions, Line Strength Values Lower State Rotational Quantum Number, Lower State Energy, and Rotational Partition Function of Each Species Observed in This Study

species	transition frequency (GHz)	line strength value (log $S\mu^2$)	lower state J	lower state energy (cm^{-1})	rotational partition function at 9.375 K (log Q)
HCN	88.631	1.43	0	0.00	1.15
HCNO	84.183	1.58	3	4.50	1.24
CH_2CN	80.479	2.69	3	4.02	2.62
CH_3CN	91.987	2.19	4	6.13	2.19
HC_3N	90.979	2.14	9	13.66	1.64
HNC	90.663	0.97	0	0.00	0.67
CH_2CO	81.586	1.36	3	13.15	1.68
HCO	86.708	0.698	0	0	1.31

Table 2. Product Branching Observed in This Study (%) Compared to Isoxazole Photodissociation Reported in Ref 35[a]

species	branching (present work)	branching (isoxazole)
HCN	50.5 (+6.4/−4.0)	53.8 (±1.7)
HCNO	18.9 (+1.8/−0.8)	
CH_2CN	11.7 (+0.8/−0.3)	7.8 (±2.9)
CH_3CN	7.4 (+1.2/−0.7)	23.4 (±6.8)
HC_3N	6.2 (+2.6/−2.1)	0.9 (±0.2)
HNC	2.3 (+0.3/−0.2)	0.9 (±0.2)
CH_2CO	1.3 (+0.5/−0.4)	3.8 (±0.9)
HCO	1.8 (+0.2/−0.1)	9.5 (±2.3)

[a]Uncertainty is dominated by systematics as discussed and quoted values estimated at 1σ.

Goldsmith's interaction potential calculations at the CASPT2 level show that nitrosopropyne has a more attractive potential at $2 < r < 5$ Å separations, which is where the dynamical bottleneck is most likely to occur. However, the available pathways for nitrosopropyne are isomerization into nitrosoallene and/or IM6 with barrier heights of 19.3 and 98.2 kJ/mol, respectively.

According to these calculations the critical hub for the bimolecular products is nitrosoallene. The calculations of Wang et al. indicate that HCN and CH_2COO form from nitrosoallene, whereas Goldsmith suggests that numerous products arise from nitrosoallene. In our CPUF experiment, the major product observed in the NO + C_3H_3 reaction is HCN (50%). As reported by Wang et al., the HCN forms from nitrosoallene through TS2, IM3, and TS3 (Green pathway in Figure 4). At low pressures, the HCN channel dominates over the temperature range 200−1000 K, and branching is always greater than 60%. However, their calculations reveal that branching for HCN is insignificant at high pressures. Goldsmith's calculations also show a pathway similar to that for HCN. In addition to this, their calculations show another pathway for HCN. As illustrated in Figure 4, this process involves the formation of isoxazole (IM5) from the initial adduct nitrosoallene via TS4, IM4, and TS5 (light blue pathway). The transition state, TS6, proceeds from isoxazole through a 1,2 H-shift from the carbon adjacent to oxygen (magenta pathway), resulting in an unstable carbene intermediate that dissociates promptly to generate HCN and CH_2CO.

As we have applied the CPUF approach to study isoxazole, and it is an important minimum on this global PES, it is useful to compare the results of the two studies. In our previous study, we used 193 nm photodissociation,[35,42] which prepares electronically excited isoxazole at higher total energy than is available here. However, a significant fraction of the observed products were attributed to ground state products following internal conversion via a low-lying conical intersection. We would thus expect somewhat similar product branching as all the minima would be accessible in both systems. HCN was also observed as a major product in unimolecular photodissociation of isoxazole with similar branching compared to our observations here.[35] However, the branching for CH_2CO is nonstoichiometric with HCN in both cases. This may be because of the secondary decomposition of CH_2CO product formed with high excess internal energy, as discussed below. We observed 1% branching for CH_2CO here and 4% in isoxazole. According to previous thermal decomposition studies on isoxazole,[35] the pyrolysis products are chiefly derived from the β-formylvinylnitrene biradical intermediate (TS10). We anticipate a similar behavior in our bimolecular

https://doi.org/10.1021/acs.jpca.2c01629
J. Phys. Chem. A 2022, 126, 5354−5362

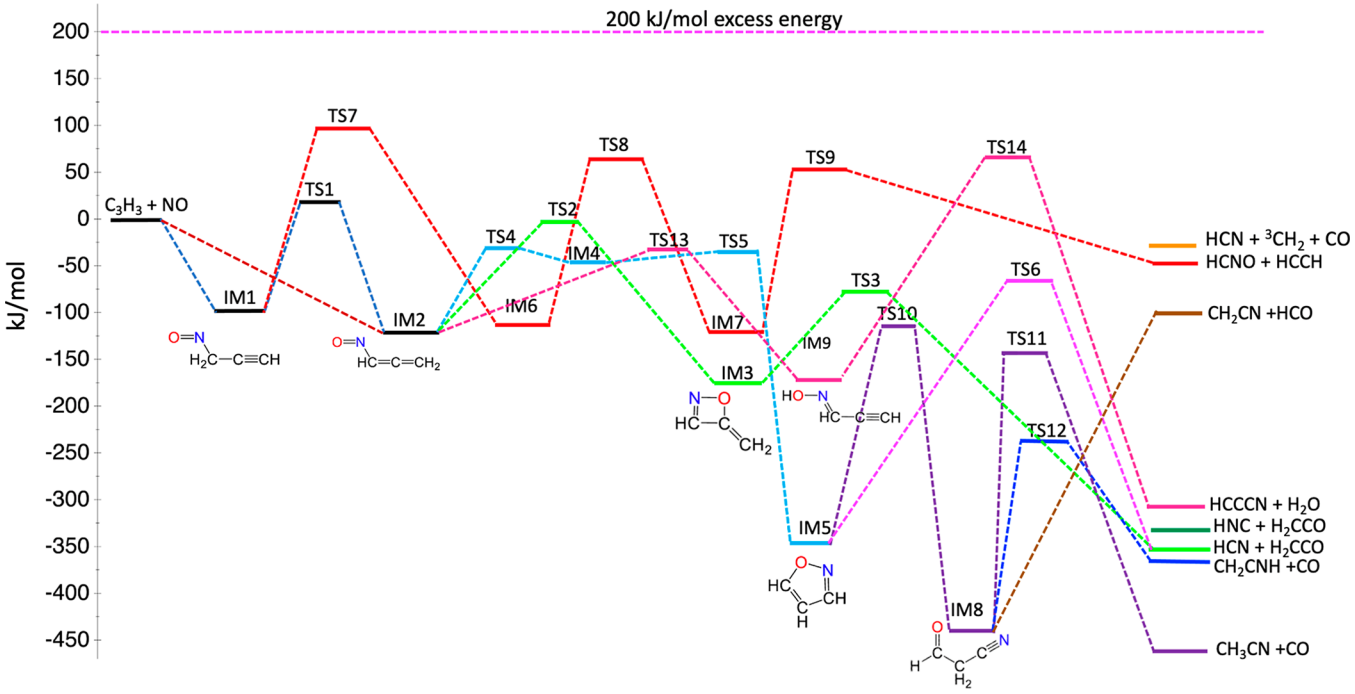

Figure 4. Key stationary points on the potential energy surface for the NO + C_3H_3 reaction. The energetics and pathways are based on high-level theoretical calculations by Wang et al. and Danilack and Goldsmith from refs 30 and 31, respectively. Table S1 in the Supporting Information contains the structures and energies for these stationary points.

reaction, in which the adducts are formed with considerable excess energy.

The second most abundant species we observed in our bimolecular reaction is HCNO (19%). According to the potential energy surface calculations by Wang et al., HCNO can formed from nitrosopropyne through a transition state located 98.2 kJ/mol above the reactants. As noted above, because of the initial internal energy in propargyl, the initial adducts may be formed with high excess energy. According to Wang's potential energy surface, HCNO may be formed from nitrosopropyne via TS7, IM6, TS8, IM7, and TS9 (red pathway). The coproduct HCCH is not detectable in our study because of the absence of a dipole moment. However, this pathway involves a series of high barriers that make the observed branching implausible. Moreover, as shown in Table 1, this channel was not seen in our isoxazole study. An alternative explanation is reaction of triplet methylene formed from secondary decomposition of ketene with the abundant NO present. This reaction is fast and barrierless.[43] If this yield is combined with that for the observed ketene, closer agreement with the HCN branching is observed. The absence of NO in the isoxazole study explains why HCNO was not observed in that case.

The third most abundant channel we observe in the present study is CH_2CN (12%) + HCO. The HCO signal we observed here is nonstoichiometric with its coproduct CH_2CN. We observed 1.9% branching for HCO, and we believe this radical can readily decompose with excess energy or react with other species in the medium to alter the detected yield. This channel was not observed in any theoretical report on the NO + C_3H_3 system. However, in our isoxazole photodissociation study, we observed this channel with comparable yields. Following isomerization of isoxazole via the β-formylvinylnitrene intermediate (TS10), formyl nitrile (IM8) is formed. This is the global minimum on the PES. HCO and CH_2CN can then be formed directly by C−C fission from IM8.

Following the first three most abundant channels, the fourth is CH_3CN (7.4%) + CO. The rotational frequencies of CO are outside of our spectral range so we were unable to detect and quantify it. According to the potential energy surface by Goldsmith, this is also from formyl nitrile (IM8), which decomposes to CH_3CN + CO through TS11 (purple pathway). This was discovered to be a major product of the thermal decomposition of isoxazole in shock tube experiments.[44] We observed CH_3CN as the second most abundant species in our photodissociation study. There, we ascribed the formation of CH_3CN to a mechanism similar to the one described above.

The formyl nitrile can also decompose to CH_2CNH + CO via TS12 (dark blue pathway). However, we have not observed the product CH_2CNH in either our photodissociation or reaction studies. Nunes et al. observed this as a major product in their flash-vacuum pyrolysis study.[36] The barrier for the formation of CH_2CNH + CO is lower than that of CH_3CN + CO. Furthermore, because the transition state frequencies for TS 12 are higher than those for TS 11, the formation of CH_3CN + CO is more favorable. In contrast to photodissociation and thermal decomposition, relatively less energy is available in flash-vacuum pyrolysis; hence, the lowest energy pathway takes precedence. Because here the adducts are formed with considerable excess energy, the high-energy path may become important, resulting in the formation of the more stable CH_3CN. In addition, isomerization of CH_2CNH to CH_3CN may occur although given the high barrier, 357 kJ/mol,[45,46] this seems less likely.

The two final product channels observed in this work are the formation of HCCCN (6.2%) with assumed cofragment, H_2O (not detected here), and HNC (2.3%), which is involved with CH_2CO. In our photodissociation study, we also observed

https://doi.org/10.1021/acs.jpca.2c01629
J. Phys. Chem. A 2022, 126, 5354−5362

these two products. According to Goldsmith, HCCCN + H_2O can be formed from IM2 via TS13, IM9, and TS14 (dark fuchsia pathway). Here TS14 is located 69 kJ/mol higher in energy than the reactants. With the excess energy that the reactant molecules possess, we believe that this barrier can be overcome to yield the desired products. However, there have been no computational reports on the HNC product channel in the NO + C_3H_3 reaction. There is a possibility of isomerization of hot HCN to HNC. The isomerization of HCN to HNC proceeds with highly excited bending states and a barrier of 187 kJ/mol.[47] At the energy of the reaction, it is likely that both are formed, and a fraction is quenched to the HNC side of the barrier.

We also found two vibrationally excited HCN products as shown in Figure 3b. Interestingly, these show maxima earlier than the corresponding ground vibrational state HCN products, suggesting there is vibrational cooling taking place in the high-density region at the throat of the nozzle. In general, vibrational cooling is far less efficient than rotational cooling, but there may be upward of 10^4 collisions with helium.

Finally, we discuss the other possible reactions that could occur in the high-density part of the flow. Wang et al. calculated the possibility of H abstraction by NO but found no H abstraction channels. We have searched the species HNO, but we did not find any lines corresponds to this. As previously mentioned, the propargyl radical can absorb a second photon and dissociate to produce C_3H_2 isomers (mainly c-C_3H_2) and H atoms. In theory, these C_3H_2 isomers can react with NO, and one major product channel would likely be the production of HNO. As mentioned earlier, we do not detect HNO. Additionally, in the high-density region, these H atoms can recombine with C_3H_2 isomers to produce propargyl, resulting in a lower amount of C_3H_2 in the medium for the bimolecular reaction. This was discussed in our previous study on propargyl photodissociation. H atoms in this region can also react with propargyl radicals to form propyne. This was discovered in an earlier study. Zhao et al. investigated the propargyl radical self-reaction and discovered that it produces benzene and three other isomers. The widely discussed propargyl self-reaction is possible here but will not lead to our detected products, all of which contain either N or O. Although all these side reactions mentioned above are possible, we believe that the NO/C_3H_3 reaction dominates in our reaction medium, leading to the products we have observed.

Photochemical models developed by Dobrijevic et al. and Hébrard et al. suggest that there is a significant mole fraction of NO and propargyl in Titan's upper atmosphere where they are formed.[27,28] These species can undergo complex reactions that result in the formation of polyatomic species. The title reaction may be important because it can couple the N and O chemistry. The presence of O and N atoms can also promote the formation of much larger N- and O-substituted polyatomic hydrocarbons in Titan's atmosphere. The above photochemical model also predicts a significant mole fraction of HNCO (isocyanic acid) in Titan's atmosphere. However, we did not observe HNCO in this study. Instead, we observed its isomer HCNO, although it is ascribed to the reaction of CH_2 with NO. Moreover, the adducts formed here, particularly IM1, IM2, IM9, IM8, and the heterocyclic compound IM5, can be stabilized by collisions in a dense atmosphere like Titan's. Finally, NO + C_3H_3 can undergo radiative association reactions to produce the aforementioned adducts.[48]

CONCLUSION

In this study, CP-FTmmW spectroscopy in a quasi-uniform flow condition was used to investigate the bimolecular radical−radical reaction NO + C_3H_3. This is another example where we showcase the power of the CPUF technique to directly and simultaneously characterize a bimolecular reaction that has several distinct products. We obtained branching for eight different observed products in this study and interpreted the dynamics guided by previous theoretical calculations and our own work on isoxazole photodissociation. This study further demonstrates that the excess internal energy in the initial reactants may play a crucial role in the reaction dynamics. With this initial excess energy, reaction channels with relatively low barriers can proceed and yield bimolecular products even at low temperatures. The title reaction can be a potential sink for the propargyl radical especially in Titan's atmosphere and similar environments.

ASSOCIATED CONTENT

Supporting Information

The Supporting Information is available free of charge at https://pubs.acs.org/doi/10.1021/acs.jpca.2c01629.

The energies and geometries of both the transition states and intermediates in Figure 4 (PDF)

AUTHOR INFORMATION

Corresponding Author

Arthur G. Suits − *Department of Chemistry, University of Missouri, Columbia, Missouri 65211, United States;* orcid.org/0000-0001-5405-8361; Email: suitsa@missouri.edu

Authors

Nureshan Dias − *Department of Chemistry, University of Missouri, Columbia, Missouri 65211, United States*

Ranil M. Gurusinghe − *Department of Chemistry, University of Missouri, Columbia, Missouri 65211, United States*

Complete contact information is available at: https://pubs.acs.org/10.1021/acs.jpca.2c01629

Notes

The authors declare no competing financial interest.

ACKNOWLEDGMENTS

This work was supported by the NSF under award CHE-1955239.

REFERENCES

(1) Lee, Y. T. Molecular beam studies of elementary chemical processes (Nobel lecture). *Angew. Chem. Int. Ed* **1987**, *26* (10), 939−951.

(2) Daranlot, J.; Jorfi, M.; Xie, C.; Bergeat, A.; Costes, M.; Caubet, P.; Xie, D.; Guo, H.; Honvault, P.; Hickson, K. M. Revealing atom-radical reactivity at low temperature through the N+ OH reaction. *Science* **2011**, *334* (6062), 1538−1541.

(3) Toscano, J.; Rennick, C. J.; Softley, T. P.; Heazlewood, B. R. A magnetic guide to purify radical beams. *J. Chem. Phys.* **2018**, *149* (17), 174201.

(4) Kaiser, R. I.; Parker, D. S. N.; Mebel, A. M. Reaction dynamics in astrochemistry: Low-temperature pathways to polycyclic aromatic hydrocarbons in the interstellar medium. *Annu. Rev. Phys. Chem.* **2015**, *66*, 43−67.

(5) Liu, K. Crossed-beam studies of neutral reactions: State-specific differential cross sections. *Annu. Rev. Phys. Chem.* **2001**, *52* (1), 139−164.
(6) Casavecchia, P.; Balucani, N.; Volpi, G. G. Crossed-beam studies of reaction dynamics. *Annu. Rev. Phys. Chem.* **1999**, *50* (1), 347−376.
(7) Smith, I. W. M.; Rowe, B. R. Reaction kinetics at very low temperatures: laboratory studies and interstellar chemistry. *Acc. Chem. Res.* **2000**, *33* (5), 261−268.
(8) Smith, I. W. M. Reactions at very low temperatures: gas kinetics at a new frontier. *Angew. Chem. Int. Ed* **2006**, *45* (18), 2842−2861.
(9) Potapov, A.; Canosa, A.; Jiménez, E.; Rowe, B. Uniform supersonic chemical reactors: 30 years of astrochemical history and future challenges. *Angew. Chem. Int. Ed* **2017**, *56* (30), 8618−8640.
(10) Kaiser, R. I.; Sun, W.; Suits, A. G.; Lee, Y. T. Crossed beam reaction of atomic carbon, C (3 P j), with the propargyl radical, C 3 H 3 (X 2 B 2): Observation of diacetylene, C 4 H 2 (X 1 Σ g+). *J. Chem. Phys.* **1997**, *107* (20), 8713−8716.
(11) Gu, X.; Kaiser, R. I. Reaction dynamics of phenyl radicals in extreme environments: a crossed molecular beam study. *Acc. Chem. Res.* **2009**, *42* (2), 290−302.
(12) Leonori, F.; Balucani, N.; Capozza, G.; Segoloni, E.; Stranges, D.; Casavecchia, P. Crossed beam studies of radical-radical reactions: O (3 P)+ C 3 H 5 (allyl). *Phys. Chem. Chem. Phys.* **2007**, *9* (11), 1307−1311.
(13) Balucani, N.; Leonori, F.; Bergeat, A.; Petrucci, R.; Casavecchia, P. Crossed-beam dynamics studies of the radical-radical combustion reaction O (3 P)+ CH 3 (methyl). *Phys. Chem. Chem. Phys.* **2011**, *13* (18), 8322−8330.
(14) Kaiser, R. I.; Le, T. N.; Nguyen, T. L.; Mebel, A. M.; Balucani, N.; Lee, Y. T.; Stahl, F.; Schleyer, P. v. R.; Schaefer, H. F., Iii A combined crossed molecular beam and ab initio investigation of C 2 and C 3 elementary reactions with unsaturated hydrocarbons—pathways to hydrogen deficient hydrocarbon radicals in combustion flames. *Faraday Discuss.* **2001**, *119*, 51−66.
(15) Kaiser, R. I.; Stranges, D.; Bevsek, H. M.; Lee, Y. T.; Suits, A. G. Crossed-beam reaction of carbon atoms with hydrocarbon molecules. IV. Chemical dynamics of methylpropargyl radical formation, C4H5, from reaction of C (3Pj) with propylene, C3H6 (X 1A). *J. Chem. Phys.* **1997**, *106* (12), 4945−4953.
(16) Alagia, M.; Balucani, N.; Casavecchia, P.; Stranges, D.; Volpi, G. G. Crossed beam studies of four-atom reactions: The dynamics of OH+ CO. *J. Chem. Phys.* **1993**, *98* (10), 8341−8344.
(17) Leonori, F.; Hickson, K. M.; Le Picard, S. D.; Wang, X.; Petrucci, R.; Foggi, P.; Balucani, N.; Casavecchia, P. Crossed-beam universal-detection reactive scattering of radical beams characterized by laser-induced-fluorescence: the case of C2 and CN. *Mol. Phys.* **2010**, *108* (7−9), 1097−1113.
(18) Casavecchia, P.; Leonori, F.; Balucani, N.; Petrucci, R.; Capozza, G.; Segoloni, E. Probing the dynamics of polyatomic multichannel elementary reactions by crossed molecular beam experiments with soft electron-ionization mass spectrometric detection. *Phys. Chem. Chem. Phys.* **2009**, *11* (1), 46−65.
(19) Rowe, B.; Dupeyrat, G.; Marquette, J.; Smith, D.; Adams, N.; Ferguson, E. The reaction O+ 2+ CH4→ CH3O+ 2+ H studied from 20 to 560 K in a supersonic jet and in a SIFT. *J. Chem. Phys.* **1984**, *80* (1), 241−245.
(20) Rowe, B. R.; Dupeyrat, G.; Marquette, J. B.; Gaucherel, P. Study of the reactions N+ 2+ 2N2→ N+ 4+ N2 and O+ 2+ 2O2→ O + 4+ O2 from 20 to 160 K by the CRESU technique. *J. Chem. Phys.* **1984**, *80* (10), 4915−4921.
(21) Sims, I. R.; Smith, I. W. M. Gas-phase reactions and energy transfer at very low temperatures. *Annu. Rev. Phys. Chem.* **1995**, *46* (1), 109−138.
(22) Sims, I. R.; Queffelec, J. L.; Defrance, A.; Rebrion-Rowe, C.; Travers, D.; Rowe, B. R.; Smith, I. W. M. Ultra-low temperature kinetics of neutral-neutral reactions: The reaction CN+ O2 down to 26 K. *J. Chem. Phys.* **1992**, *97* (11), 8798−8800.
(23) Carty, D.; Goddard, A.; Köhler, S. P.; Sims, I. R.; Smith, I. W. Kinetics of the Radical- Radical Reaction, O (3P J)+ OH (X2ΠΩ)→ O2+ H, at Temperatures down to 39 K. *J. Phys. Chem. A* **2006**, *110* (9), 3101−3109.
(24) Hickson, K. M.; Bergeat, A. Low temperature kinetics of unstable radical reactions. *Phys. Chem. Chem. Phys.* **2012**, *14* (35), 12057−12069.
(25) Bergeat, A.; Daranlot, J.; Hickson, K. M.; Costes, M. Interstellar chemistry of atomic nitrogen: Low temperature kinetics of the N+ OH, N+ CN and N+ NO reactions. *EAS Publ. Ser.* **2012**, *58*, 283−286.
(26) Gurusinghe, R. M.; Dias, N.; Mebel, A. M.; Suits, A. G. Radical-Radical Reaction Dynamics Probed Using Millimeterwave Spectroscopy: Propargyl+ NH2/ND2. *J. Phys. Chem. Lett.* **2022**, *13*, 91−97.
(27) Hébrard, E.; Dobrijevic, M.; Loison, J.-C.; Bergeat, A.; Hickson, K. M.; Caralp, F. Photochemistry of C3Hp hydrocarbons in Titan's stratosphere revisited. *Astron. Astrophys.* **2013**, *552*, A132.
(28) Dobrijevic, M.; Hébrard, E.; Loison, J. C.; Hickson, K. M. Coupling of oxygen, nitrogen, and hydrocarbon species in the photochemistry of Titan's atmosphere. *Icarus* **2014**, *228*, 324−346.
(29) DeSain, J. D.; Hung, P. Y.; Thompson, R. I.; Glass, G. P.; Scuseria, G.; Curl, R. F. Kinetics of the reaction of propargyl radical with nitric oxide. *J. Phys. Chem. A* **2000**, *104* (15), 3356−3363.
(30) Wang, X.; Song, J.; Lv, G.; Li, Z. Theoretical study on the reaction of nitric oxide with propargyl radical. *J. Phys. Chem. A* **2019**, *123* (5), 1015−1021.
(31) Danilack, A. D.; Goldsmith, C. F. A computational investigation into the kinetics of NO+ CH2CCH and its effect on NO reduction. *Proc. Combust Inst* **2019**, *37* (1), 687−694.
(32) Broderick, B. M.; Suas-David, N.; Dias, N.; Suits, A. G. Isomer-specific detection in the UV photodissociation of the propargyl radical by chirped-pulse mm-wave spectroscopy in a pulsed quasi-uniform flow. *Phys. Chem. Chem. Phys.* **2018**, *20* (8), 5517−5529.
(33) Gurusinghe, R. M.; Dias, N.; Krueger, R.; Suits, A. G. Uniform supersonic flow sampling for detection by chirped-pulse rotational spectroscopy. *J. Chem. Phys.* **2022**, *156* (1), 014202.
(34) Abeysekera, C.; Joalland, B.; Ariyasingha, N.; Zack, L. N.; Sims, I. R.; Field, R. W.; Suits, A. G. Product branching in the low temperature reaction of CN with propyne by chirped-pulse microwave spectroscopy in a uniform supersonic flow. *J. Phys. Chem. Lett.* **2015**, *6* (9), 1599−1604.
(35) Dias, N.; Joalland, B.; Ariyasingha, N. M.; Suits, A. G.; Broderick, B. M. Direct versus indirect photodissociation of isoxazole from product branching: A chirped-pulse Fourier transform mm-wave spectroscopy/pulsed uniform flow investigation. *J. Phys. Chem. A* **2018**, *122* (38), 7523−7531.
(36) Nunes, C. M.; Reva, I.; Pinho e Melo, T. M.; Fausto, R.; Solomek, T.; Bally, T. The pyrolysis of isoxazole revisited: A new primary product and the pivotal role of the vinylnitrene. A low-temperature matrix isolation and computational study. *J. Am. Chem. Soc.* **2011**, *133* (46), 18911−18923.
(37) Oldham, J. M.; Abeysekera, C.; Joalland, B.; Zack, L. N.; Prozument, K.; Sims, I. R.; Park, G. B.; Field, R. W.; Suits, A. G. A chirped-pulse Fourier-transform microwave/pulsed uniform flow spectrometer. I. The low-temperature flow system. *J. Chem. Phys.* **2014**, *141* (15), 154202.
(38) Foley, C. D.; Alavi, S. T.; Joalland, B.; Broderick, B. M.; Dias, N.; Suits, A. G. Imaging the infrared multiphoton excitation and dissociation of propargyl chloride. *Phys. Chem. Chem. Phys.* **2019**, *21* (3), 1528−1535.
(39) Lee, Y.-R.; Lin, S.-M. Photodissociation of CH≡ CCH 2 X (X= Br and Cl) by translational spectroscopy. *J. Chem. Phys.* **1998**, *108* (1), 134−141.
(40) Robinson, J. C.; Sun, W.; Harris, S. A.; Qi, F.; Neumark, D. M. Photofragment translational spectroscopy of 1, 2-butadiene at 193 nm. *J. Chem. Phys.* **2001**, *115* (18), 8359−8365.
(41) Müller, H. S. P.; Schlöder, F.; Stutzki, J.; Winnewisser, G. The Cologne Database for Molecular Spectroscopy, CDMS: a useful tool for astronomers and spectroscopists. *J. Mol. Struct.* **2005**, *742* (1−3), 215−227.

https://doi.org/10.1021/acs.jpca.2c01629
J. Phys. Chem. A 2022, 126, 5354−5362

(42) Cao, J. Photoinduced reactions of both 2-formyl-2 H-azirine and isoxazole: A theoretical study based on electronic structure calculations and nonadiabatic dynamics simulations. *J. Chem. Phys.* **2015**, *142* (24), 244302.
(43) Fikri, M.; Meyer, S.; Roggenbuck, J.; Temps, F. An experimental and theoretical study of the product distribution of the reaction CH 2 (X [combining tilde] 3 B 1)+ NO. *Faraday Discuss.* **2001**, *119*, 223−242.
(44) Lifshitz, A.; Wohlfeiler, D. Thermal decomposition of isoxazole: experimental and modeling study. *J. Phys. Chem.* **1992**, *96* (11), 4505−4515.
(45) Cho, H.-G. Matrix Infrared Spectra and DFT Computations of CH 2 CNH and CH 2 NCH Produced from CH 3 CN by Laser-Ablation Plume Radiation. *Bull. Korean Chem. Soc.* **2013**, *34* (5), 1361−1365.
(46) Mencos, A.; Krim, L. Isomerization and fragmentation of acetonitrile upon interaction with N (4S) atoms: the chemistry of nitrogen in dense molecular clouds. *Mon. Not. R. Astron. Soc.* **2016**, *460* (2), 1990−1998.
(47) Lee, T. J.; Rendell, A. P. The structure and energetics of the HCN → HNC transition state. *Chem. Phys. Lett.* **1991**, *177* (6), 491−497.
(48) Vuitton, V.; Yelle, R. V.; Lavvas, P.; Klippenstein, S. J. Rapid association reactions at low pressure: Impact on the formation of hydrocarbons on Titan. *Astrophys. J.* **2012**, *744* (1), 11.

https://doi.org/10.1021/acs.jpca.2c01629
J. Phys. Chem. A 2022, 126, 5354−5362